International Journal of Modern Manufacturing Technologies
ISSN 2067–3604, Vol. XVII, No. 2 / 2025
https://doi.org/ 10.54684/ijmmt.2025.17.2.23

INTEGRATION OF BIONICS AND NUMERICAL SIMULATIONS IN THE DESIGN OF A LIGHTWEIGHT AND HIGH-STIFFNESS MACHINE TOOL BODY

Krzysztof Lehrich[1]

[1] Silesian University of Technology, Faculty of Mechanical Engineering, Department of Machine Technology
Konarskiego 18A, 44-100 Gliwice, Poland

Corresponding author: Krzysztof Lehrich, krzysztof.lehrich@polsl.pl

Abstract: Designing machine tool bodies requires consideration of high structural stiffness, reduced mass, and stability under operational loads. This article presents a concept for a milling headstock inspired by biological structures such as the beak of a toucan and a woodpecker, which exhibit advantageous mechanical properties. The objective of the study was to develop an alternative form of the headstock body that combines lightweight construction with high stiffness, while simultaneously increasing its natural frequencies. Topological and parametric optimization methods were employed, utilizing the MOGA algorithm and finite element analysis (FEA) tools. In addition, the shape was optimized using fig and blackberry leaf models as biological analogues, refining their geometric form to ensure effective distribution of material for load transfer. The analysis of the headstock body demonstrated improved static and dynamic performance of the optimized design compared to a conventional box-type structure. The results confirm the potential of bionic design in the development of advanced machine tool components. This study highlights the importance of integrating biological inspiration with advanced engineering methodologies in the design process.

Key words: bionic design, topological optimization, headstock, machine tool body, structural stiffness, evolutionary algorithms

1. INTRODUCTION

The structural components of machine tools play a critical role in maintaining machining accuracy over extended periods of operation. Their design directly influences the system's stability, stiffness, vibration resistance, and thermal expansion predictability. In industrial practice, machine tool bodies are typically designed based on proven solutions. Designers tend to follow established requirements and available manufacturing technologies, rarely venturing into innovative approaches due to the risk of failure. Moreover, the necessity to meet delivery deadlines often limits the adoption of novel structural concepts. Consequently, scientific research in this area may lead to unconventional design solutions with more desirable characteristics. An additional driving force is the rapid advancement of emerging technologies in recent years, such as 3D printing and AI-based engineering tools, which offer new opportunities for innovation in machine tool design.

This article explores a headstock body design inspired by bionic principles. Bionic design, which inherently integrates knowledge from biology, engineering, mathematics, and computer science [1,2], has been successfully applied across a wide range of technical domains. These include:

- The development of novel materials and structures, such as ultra-lightweight and high-strength materials inspired by bird bones or insect exoskeletons [3,4], and cutting tools modeled after animal teeth [5].
- Performance optimization of devices, for example, low-friction surface coatings inspired by shark skin [6,7], turbine blades with enhanced cooling efficiency modeled after fan palm leaves [8], and maneuverable robots mimicking fish locomotion [9,10].
- The advancement of vibration-damping systems based on the anatomical structure of a woodpecker's head [11,12].
- The development of control systems and robotics, such as walking robots that replicate the morphology and gait of animals [13,14].

The essence of bionic design lies in the deliberate process of drawing inspiration from nature and replicating its examples and mechanisms [15]. Researchers and engineers observe how nature has solved complex problems and attempt to emulate these solutions [1]. Living organisms have evolved optimal body structures to adapt to their

environments [7], making them ideal prototypes for bionic applications [5,16].
Authors working within the field of bionic design emphasize that it does not involve direct one-to-one replication of natural forms, as this is often technically unfeasible and inefficient [1]. This limitation arises from the fact that natural structures and materials are highly complex, frequently exhibiting hierarchical, multiscale, and composite architectures. Therefore, it is essential to understand the underlying principles of biological solutions and then abstract and adapt them for engineering applications [1]. Effective design outcomes result from an appropriately chosen level of abstraction [1] - a deliberate process of simplifying, generalizing, and modifying complex natural structures, mechanisms, and principles to enable their successful implementation in technical systems. This process requires translating observed biological phenomena into functional equivalents that can be applied within artificial environments [2].
The process of adapting natural prototypes for technical applications is largely constrained by existing technological limitations. Bionic solutions are often too complex for direct implementation [1]. Bioinspired internal structures are frequently difficult to manufacture using conventional technologies [1,17]. Many living organisms integrate multiple functions into a single component. For example, beetle wings (elytra) serve simultaneously as protective, load-bearing, and thermoregulatory elements. Replicating such multifunctionality in artificial materials remains a significant challenge [3]. Additional manufacturing issues arise, such as limited resolution in 3D printing [1], which affects the accuracy of reproducing complex structures like porous networks, tubular geometries [1], or spider web-inspired designs [17]. Moreover, 3D printing introduces further complications related to dimensional precision, which can result in assembly clearances, mechanical jamming, and ultimately malfunctioning systems [18]. These difficulties in replicating natural designs often necessitate the use of additional components, such as connectors, which may compromise mechanical or thermal efficiency [4].
Researchers working on bionic structures frequently utilize simulation tools to evaluate structural behavior prior to physical prototyping. However, this approach also presents challenges. Similar to the difficulties encountered in physically replicating nature, numerical models face analogous issues - for instance, accurately representing the internal structure of bones or porous architectures [1]. Moreover, discrepancies in simulation results may arise due to the omission of factors such as surface roughness, material heterogeneity, or residual stresses [1]. A particularly demanding area involves simulations of coupled physical fields, including fluid flow, heat transfer, chemical reactions, and structural mechanics [3,19].
Biological solutions are optimized for highly specific environmental conditions, such as temperature, pressure, and humidity, which rarely align with the operational environments of technical devices. Transferring such solutions without adaptation to new conditions often fails. Moreover, significant differences in scale exist. Biology frequently operates at the micro- or nanoscale (e.g., the superhydrophobic surface of a lotus leaf), whereas engineering requires solutions applicable at the macroscale. Accurately replicating micro- and nanostructures over large surfaces is both technically challenging and economically demanding [18].
Due to the high complexity of living organisms, no universal design methodology has been developed. However, two primary approaches to bionic design can be distinguished. The first is referred to as the problem-driven approach, also known as Analogy Bionic [1,2]. This method is generally classified as a top-down approach. It is based on the premise that an engineer or designer is confronted with a specific technical problem and actively seeks inspiration from biological systems to address it [1,2]. The second approach is referred to as the bottom-up method. It is solution-driven and also known as the biology push approach [2]. The essence of this method lies in transforming an observed biological phenomenon, structure, or mechanism into a technical implementation in the form of a new product, technology, or similar application [2].
This article presents an attempt at bionically inspired FEA-based optimization of a milling headstock. The approach is grounded in the view that shape optimization using contemporary FEA tools constitutes an integral and essential component of advanced bionic design [1,2,5,16,20].

2. MATERIALS AND METHODS

The objective of topological optimization in FEA is to identify the most efficient material distribution within a defined design space to maximize specific properties - such as stiffness or strength - while minimizing material volume [19]. This tool aims to find an optimal solution to a given engineering problem, rather than replicate an existing complex form such as bionic structures [19].
Initially, this concept was illustrated using examples of fig and blackberry leaves. The Ansys system was employed to perform the topological optimization. In reality, each leaf represents a multifunctional structure optimized for numerous, often conflicting objectives. The functions of a leaf that are reflected in its structural design include: maximizing solar light absorption [15,18], efficient transport of water and nutrients [3],

temperature regulation [15], protection against environmental factors such as wind and rain [1,15], and, in some cases, self-cleaning and hydrophobicity [5,15].
The shape optimization of the leaves was focused solely on load-bearing capacity and structural strength, without accounting for their other biological functions. The leaf geometries obtained through simulation were the result of predefined volumes (Figures 1a, 2a), constrained by the external contours of their real-life counterparts, subjected to external surface loads and supported at the ends of their petioles (Figures 1c, 2c). The final shape was also influenced by regions excluded from the optimization process, including the outlines of the leaf petioles and their edge contours (Figures 1b, 2b). It is generally understood that these features are shaped by a multitude of biological, genetic, and environmental factors. The most significant factor influencing leaf shape is genetic regulation, which controls how leaf cells divide and differentiate, ultimately determining the final contour. The material distribution obtained through optimization was also affected by the FEA mesh resolution. In both models, a mesh composed of tetrahedral elements with a size of 0.5 mm was used. This resulted in 908,005 finite elements for the fig leaf model and 515,606 finite elements for the blackberry leaf model. The optimized leaf shapes obtained through simulation are shown in Figures 1e and 2e. It was observed that the vein networks in the shape-optimized models are similar but do not match their real-life counterparts (Figures 1d and 2d). This discrepancy arises from the fact that the optimization process seeks the most efficient material distribution for transferring the defined loads within the pre-established design space. The differences primarily stem from the reality that natural vein networks are optimized for fluid transport, whereas structural stiffness is a secondary function in actual leaves.

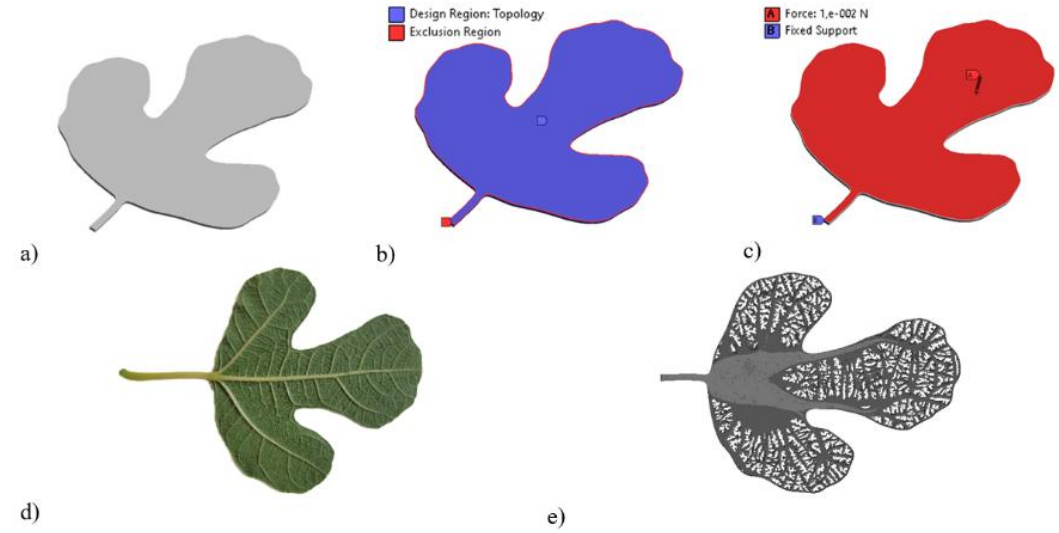

Fig. 1. Shape optimization of a fig leaf: (a) initial geometry for optimization, (b) spatial segmentation for optimization, (c) boundary conditions, (d) original fig leaf, (e) leaf shape obtained after shape optimization

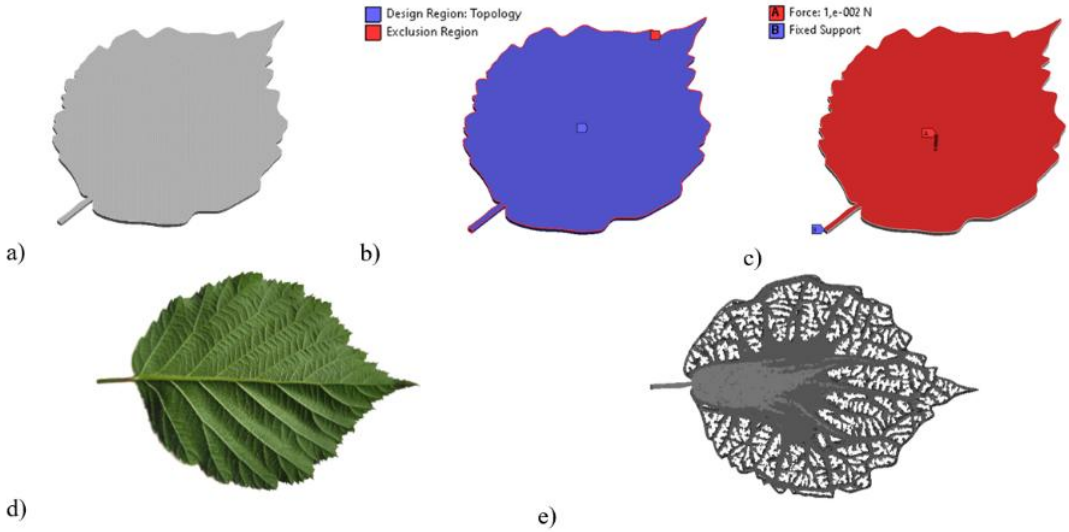

Fig. 2. Shape optimization of a blackberry leaf: (a) initial geometry for optimization, (b) spatial segmentation for optimization, (c) boundary conditions, (d) original blackberry leaf, (e) leaf shape obtained after shape optimization

Based on the numerical experiments described above, it was concluded that the definition of the initial volume and the exclusion zones from the optimization process play a critical role in determining the final shapes obtained through topological optimization. The main part of the study focused on the topological optimization of the headstock of a milling center, whose kinematics are illustrated in Figure 3.

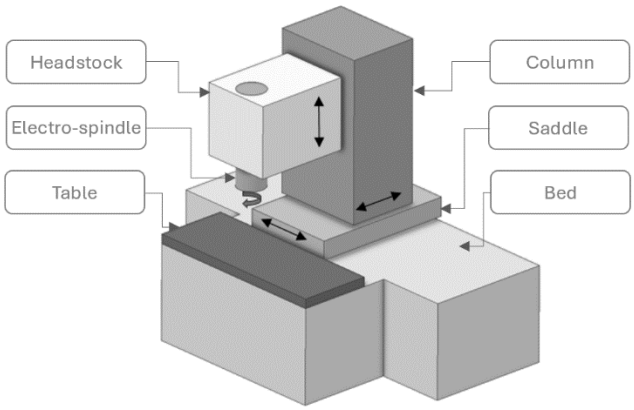

Fig. 3. General schematic of a milling center

In the context of searching for an optimal shape of the milling headstock based on bionic structures, the beaks of the toucan and woodpecker were used as reference models due to their conceptual and structural similarities. These similarities arise from the pursuit of comparable design goals: achieving maximum stiffness and strength while minimizing mass. Analogies can be drawn at the level of design objectives and construction principles that enable these biological structures to perform their functions effectively.

The toucan's beak must be lightweight to avoid burdening the bird, yet sufficiently stiff and strong to fulfill its functional roles [21,22]. Its structure serves as a natural example of optimization for a high stiffness-to-weight ratio [21]. Similarly, the headstock is designed with an emphasis on maximizing stiffness to ensure machining accuracy and suppress vibrations. At the same time, reducing its mass is a key consideration, particularly in the context of feed drive dynamics.

Thanks to its structural composition, the toucan's beak is capable of withstanding bending loads and preventing catastrophic failure, which is essential for its defensive and foraging functions [21,22]. Similarly, the headstock - like other machine tool bodies - must exhibit high stiffness to effectively transmit cutting forces with minimal deformation, thereby ensuring machining precision.

The woodpecker's beak can also serve as an inspiration for the design of a milling headstock, particularly in the context of developing structures capable of withstanding high impact loads, ensuring high stiffness, and minimizing the adverse effects of vibration-key challenges in machine tool construction. Although the headstock and the beak serve entirely different functions, the biomechanical principles underlying the strength and performance of the woodpecker's beak offer valuable analogies and solutions for mechanical engineering.

The woodpecker's beak is a natural model of an optimized, rigid load-transmitting mechanism combined with a vibration-damping system. Similarly, the headstock is responsible for the precise and efficient transmission of torque and cutting forces, while also damping vibrations generated during the machining process. This requires maximum stiffness of the entire system (spindle-holder-tool) and favorable damping properties. In the woodpecker, before impact, muscles tense the hyoid bone, increasing the natural frequency of the head [23]. As a result, the head's natural frequency is significantly higher than the impact frequency, which prevents resonance that could otherwise damage the brain [23, 24]. Avoiding resonance is likewise a critical issue in machine tool design.

Resonant vibrations lead to deterioration in the quality of the machined surface and accelerated tool wear. The design inspiration here lies in developing headstocks with high natural frequencies that significantly exceed the excitation frequencies generated during the cutting process. Given that the headstock is part of a larger dynamic system, a bionic analogy to the woodpecker suggests that engaging the entire structure in stabilizing the process is essential. The forces and vibrations generated at the tool-workpiece interface should be transmitted and dissipated throughout the entire machine structure, including the foundation.

A top-down approach was applied in the optimization of the headstock body. It was assumed that an alternative structural form was needed to replace the conventional box-type headstock (Figure 4), aiming for increased stiffness and reduced mass. Consequently, reducing the mass of the headstock while increasing its stiffness should simultaneously lead to an increase in its natural vibration frequencies.

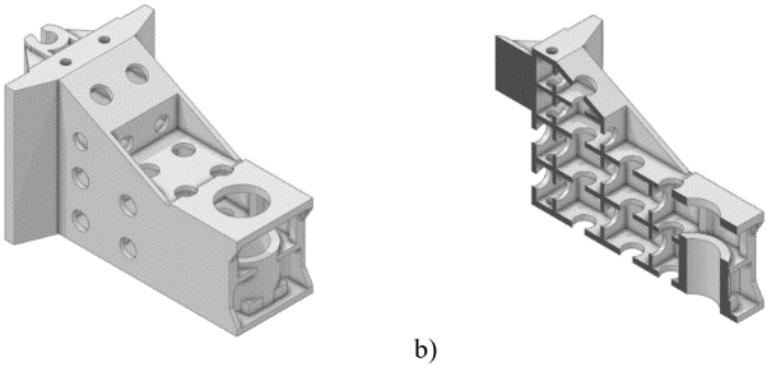

Fig. 4. Original box-type design of the spindle head: (a) general view, (b) sectional view

Based on the conclusions drawn during the preliminary research phase, the simulation model preparation began with defining the initial volume of the headstock. For this purpose, a cuboid with dimensions of 837 × 580 × 550 millimeters was adopted, encompassing the geometry of the conventional box-type headstock (Figure 5). It was assumed that the surfaces where degrees of freedom are constrained, as well as the mounting surface for the electrospindle - where external forces are applied - would be excluded from the optimization process. The arrangement of guide blocks, the mounting location for the ball nut housing, and the opening for electrospindle installation were defined analogously to their positions in the box-type design.

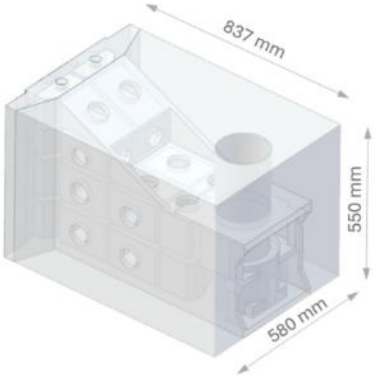

Fig. 5. Assembly of the box-type body and the input volume for optimization

At the mounting points of the guide blocks, translational movement was constrained in directions perpendicular to the feed motion of the headstock, specifically along the X and Z axes, as illustrated in Figure 6a. At the location of the ball nut housing, movement was restricted along the feed direction, i.e., the Y axis (Figure 6b). At the electrospindle mounting surface, five loading scenarios were defined (Figures 6c to 6g). Each scenario involved the independent application of a force of F = 1000 N along the X, -X, Y, and Z directions. The fifth scenario applied a torque of M = 500 Nm to the same surface. A sixth loading case involved the application of gravitational acceleration along the -Y direction (Figure 6h). Additionally, the simulation assumptions included symmetry of the headstock body in the XY plane. This allowed for a reduction in the number of loading cases and, consequently, a shortening of the simulation time.

In the input model for topological optimization, a mesh composed of tetrahedral finite elements with a size of 10 mm was used. This resulted in 2,155,328 finite elements for the cuboid primitive. The element size was selected based, among other factors, on the minimum wall thickness expected in the optimized model. Analogous boundary conditions and loading scenarios were applied to the simulation of the box-type headstock body, with the results serving as reference values for the outcomes obtained through topological optimization. In both cases, the same material was assumed - gray cast iron - with properties listed in Table 1.

Table 1. Mechanical properties of the headstock body

	Grey Cast Iron
Young's Modulus [MPa]	110000
Poisson's Ratio	0.28
Mass Density [kg/m3]	7200

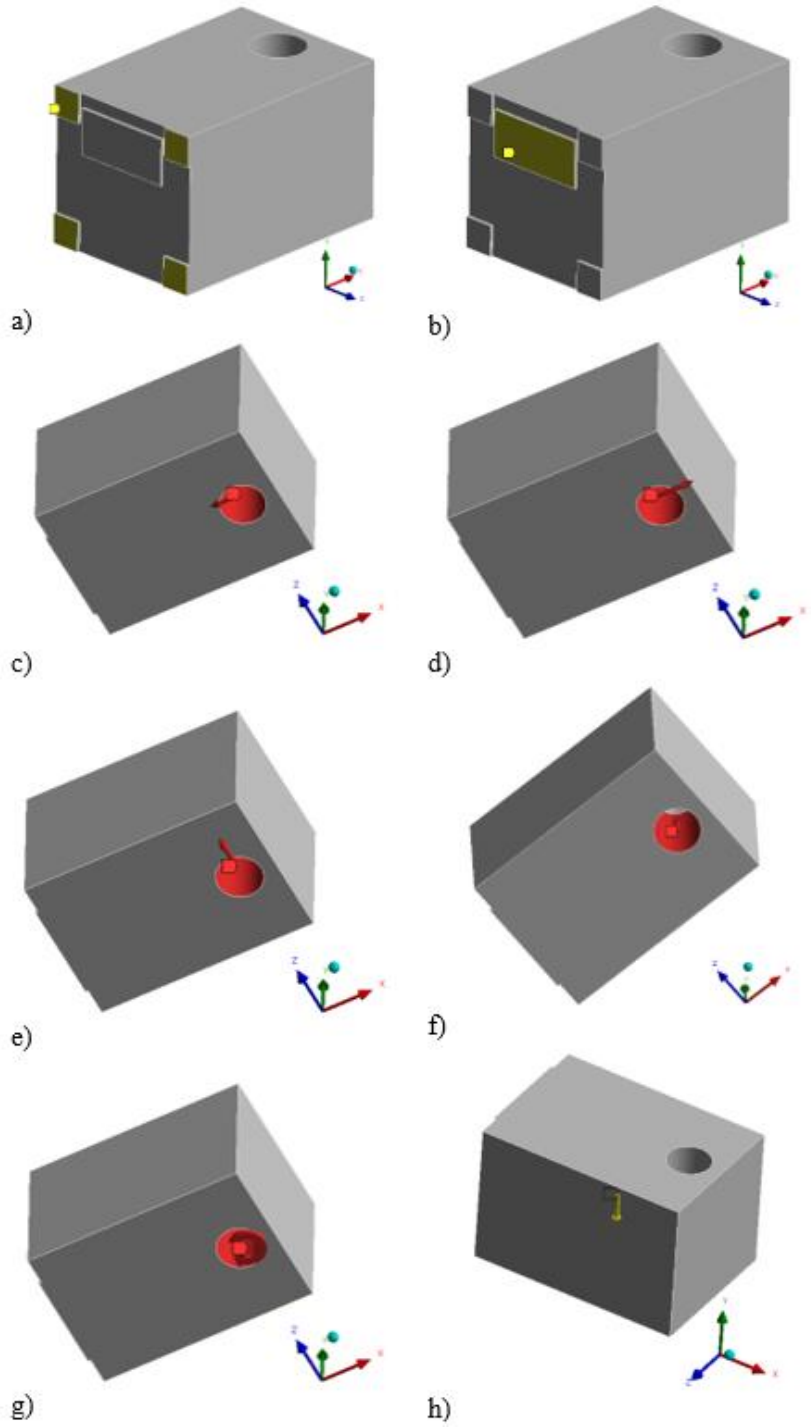

Fig. 6. Boundary conditions and loading cases: (a) displacement constraints along X and Z directions, (b) displacement constraint along Y direction, (c) force applied in the -X direction, (d) force applied in the X direction, (e) force applied in the Z direction, (f) force applied in the Y direction, (g) applied torque, (h) gravitational acceleration in the -Y direction

The results of the topological optimization served as a starting point for the next stage - parametric optimization. To facilitate this, the shape-optimized headstock model was simplified in terms of surface complexity, taking into account technological feasibility. The parametric optimization model was developed in a CAD system and further modified in the Design Modeler module of Ansys to enable parameterization. Parametric optimization was performed using the Multi-Objective Genetic Algorithm (MOGA). MOGA is a multi-criteria genetic algorithm that simulates the evolutionary process of a population of solutions. It is based on selection, crossover, and mutation, generating a set of Pareto-optimal solutions. The optimization objectives were defined as minimizing mass and maximizing static stiffness, i.e., minimizing displacements along the three axes of the adopted coordinate system. The design variables were the thicknesses of six headstock walls, shown in Figure 7 and labeled D1 through D6. It was assumed that the wall thicknesses could vary within the range of 10 to 30 millimeters.

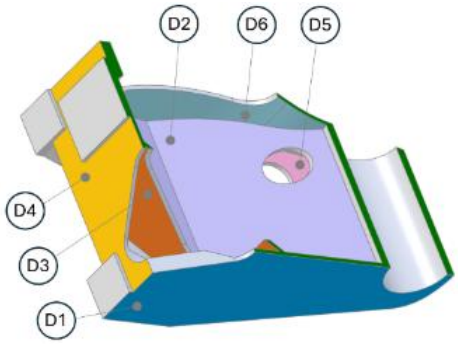

Fig. 7. Cross-section of the headstock body highlighting walls chosen for parametric optimization, identified as D1–D6: D1 – bottom wall, D2 – internal vertical rib, D3 – internal diagonal rib, D4 – rear wall, D5 – side wall, D6 – top wall

3. RESULTS AND DISCUSSIONS

In the topology optimization process, the mass of the cuboidal primitive was reduced to 20%. The procedure was carried out over 56 iterations, resulting in a geometry that resembled both a bone-like structure and the shape of a toucan's beak, which served as a source of bionic inspiration in this case (Figure 8a).
The resulting structure featured a reduced internal volume reinforced with ribs, mimicking natural load-bearing structures. Although the model ensured geometric continuity, its mass (approximately 376 kg) exceeded the reference value for the box-type headstock (340 kg). Therefore, a simplified geometric model was developed for parametric optimization (Figure 8b), which was subsequently analyzed with respect to mass minimization and static stiffness maximization.

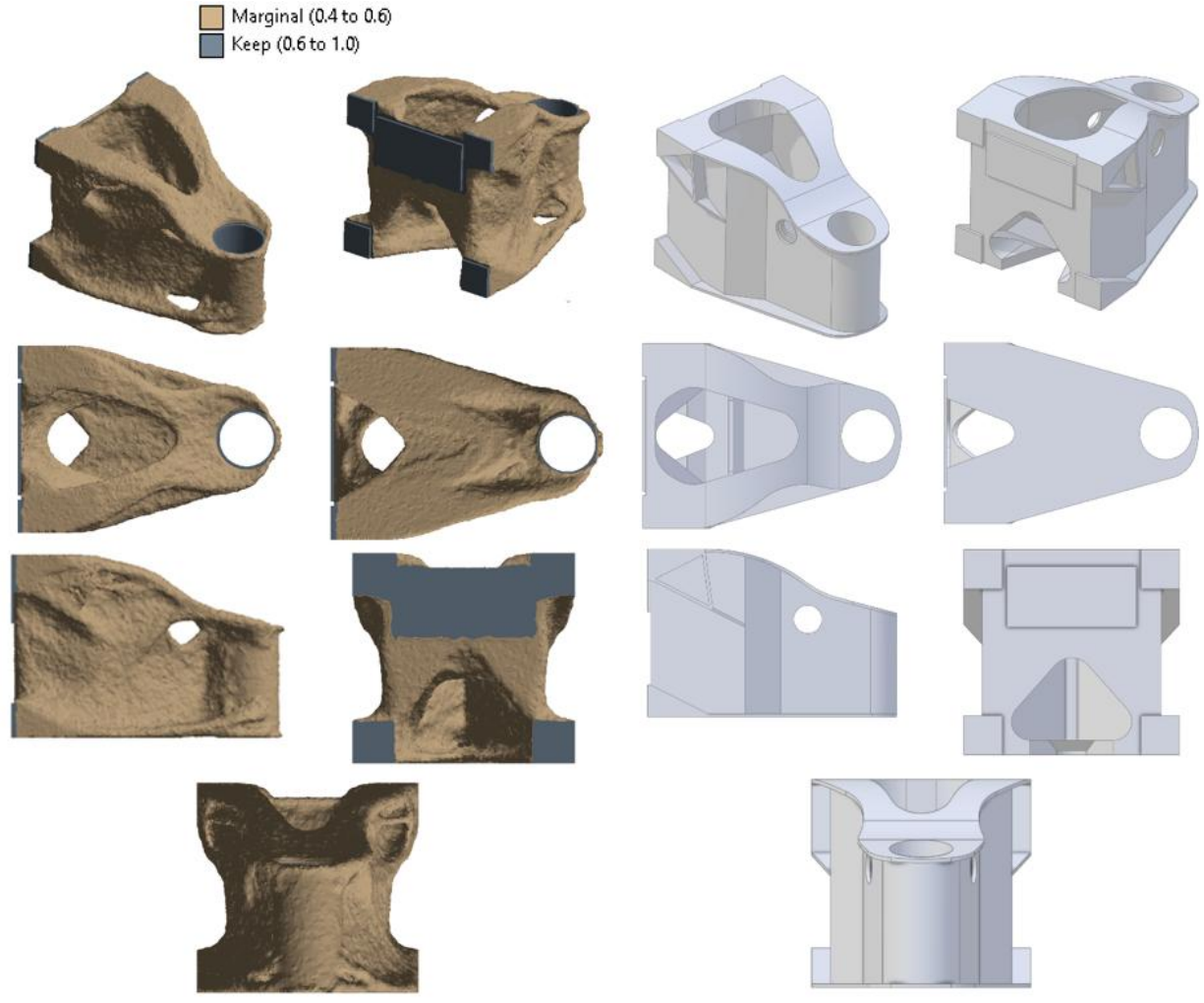

a) b)

Fig. 8. Geometry of the headstock body following topological optimization: (a) results of topological optimization performed in Ansys, (b) simplified model prepared for parametric optimization

The MOGA (Multi-Objective Genetic Algorithm) method was employed for parametric optimization, generating successive populations of solutions across iterations. Table 2 presents the three best design variants, listing the wall thicknesses (D1–D6), displacement values in the X, Y, and Z directions, and the total mass. Figure 9 illustrates the evolution of the parameters (D1–D6) across successive generations of the population.
The points shown along the X-axis represent so-called design points, i.e., successive sets of parameters (D1–D6) generated and evaluated by the solver during the optimization process. The first 100 points correspond to the exploration phase of the design space, characterized by a wide dispersion of values. In the subsequent points, a stabilization of parameter values is observed. The algorithm evaluated 400 different model variants, ultimately converging on parameter values close to the optimum.
The result of this parametric optimization process is a set of potential solutions, represented by three parameter sets (D1–D6) listed in Table 2 as "Candidate Points." These solutions originate from the Pareto front, which is characteristic of multi-objective analysis. The optimization was conducted to maximize static stiffness in the X, Y, and Z directions while minimizing mass.

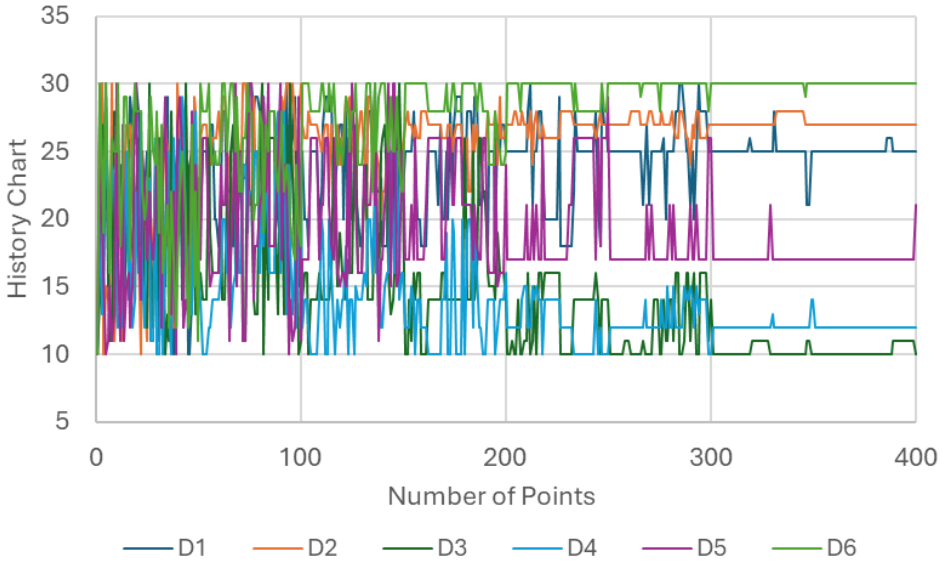

Fig. 9. History Chart of parameters D1 - D6

Table 2. Overview of results from parametric optimization

Optimization parameters		Candidate Point 1	Candidate Point 2	Candidate Point 3
D1		25	26	25
D2		27	27	27
D3		10	10	10
D4		12	12	12
D5		21	17	17
D6		30	30	30
Directional Deformation, mm	Z	0.00043	0.00044	0.00044
	Y	0.00200	0.00201	0.00202
	X	0.00275	0.00275	0.00277
Solid Mass, kg		305.1	302.2	301.0

Prioritizing mass minimization as the primary criterion, and considering the negligibly small differences in maximum displacements recorded at the spindle mounting hole, the dimensions corresponding to Candidate 3

(Table 2) were ultimately selected. The FEA displacement results for the selected set of wall thicknesses (D1–D6), under loads applied in the X, Y, and Z directions and a moment applied at the spindle mounting axis, are compared with the results obtained for the box-type headstock and presented in Figure 10.
The combined application of topological and parametric optimization enabled a reduction in headstock body mass by approximately 12%. More significantly, the displacements resulting from forces simulating spindle loading were reduced. As a result, static stiffness increased by 111% and 110% along the X and Y directions, respectively, and by 74,9% along the Z direction (Table 3). This also translated into an increase in torsional stiffness along the spindle axis (Figure 10d).

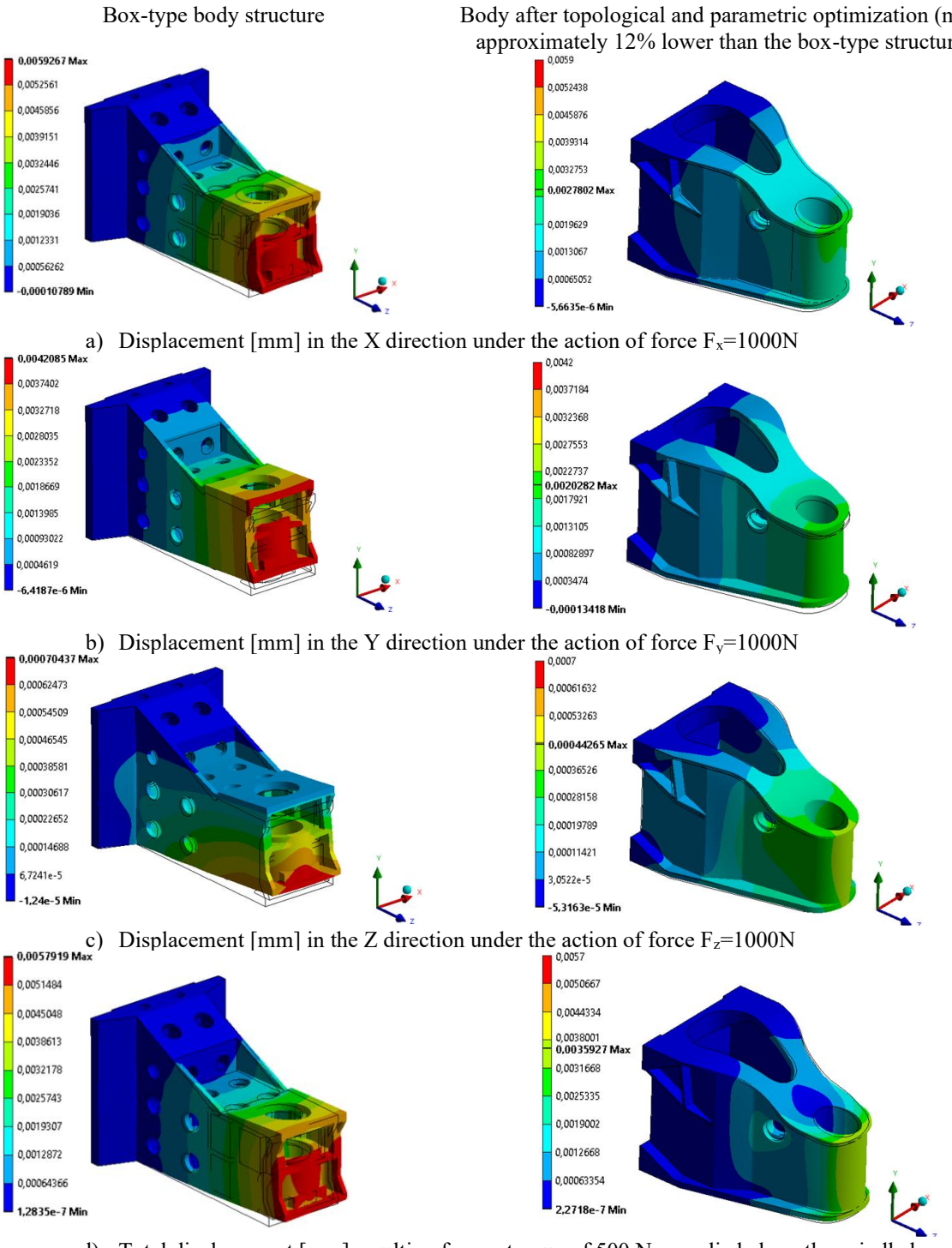

a) Displacement [mm] in the X direction under the action of force F_x=1000N

b) Displacement [mm] in the Y direction under the action of force F_y=1000N

c) Displacement [mm] in the Z direction under the action of force F_z=1000N

d) Total displacement [mm] resulting from a torque of 500 Nm applied along the spindle bore axis

Fig. 10. Comparison of displacements for the box-type structure and the designs after topological and parametric optimization: (a)(b)(c) directional displacements resulting from the action of a force in a given direction, (d) total displacements resulting from the action of a moment in the electro-spindle mounting hole

Table 3. Comparison between the box-type structure and the optimized design

Parameter		Box-type body structure	Body after topological and parametric optimization	Change in relation to the box-type body structure, %
Static Stiffness, N/μm	X	169	357	111.2
	Y	238	500	110.1
	Z	1429	2500	74.9
Mass, kg		340	301	-11.5

Additionally, a modal analysis was carried out. Figure 11 presents the first three natural frequencies and corresponding mode shapes, comparing the box-type structure with the design after topological and parametric optimization. The mode shapes are visualized using color gradients and numerical indicators in the legend to facilitate interpretation of each vibration mode. These numerical values do not represent actual displacements in physical units, as the modal finite element analysis does not account for external forces or damping. The displacement magnitudes are scaled independently for each mode by the solver, making direct comparisons between modes infeasible. Nevertheless, the vibration shapes remain consistent across configurations. Notably, due to increased stiffness and reduced mass, the first two natural frequencies rose by 38% for the first mode (Fig. 11a) and 34% for the second (Fig. 11b), which is advantageous for machine tool performance. These two modes exhibit bending behavior aligned with the force directions considered during the optimization process. The third mode displays a torsional character, and in this case, the vibration frequencies of the box-type and optimized structures are very similar.

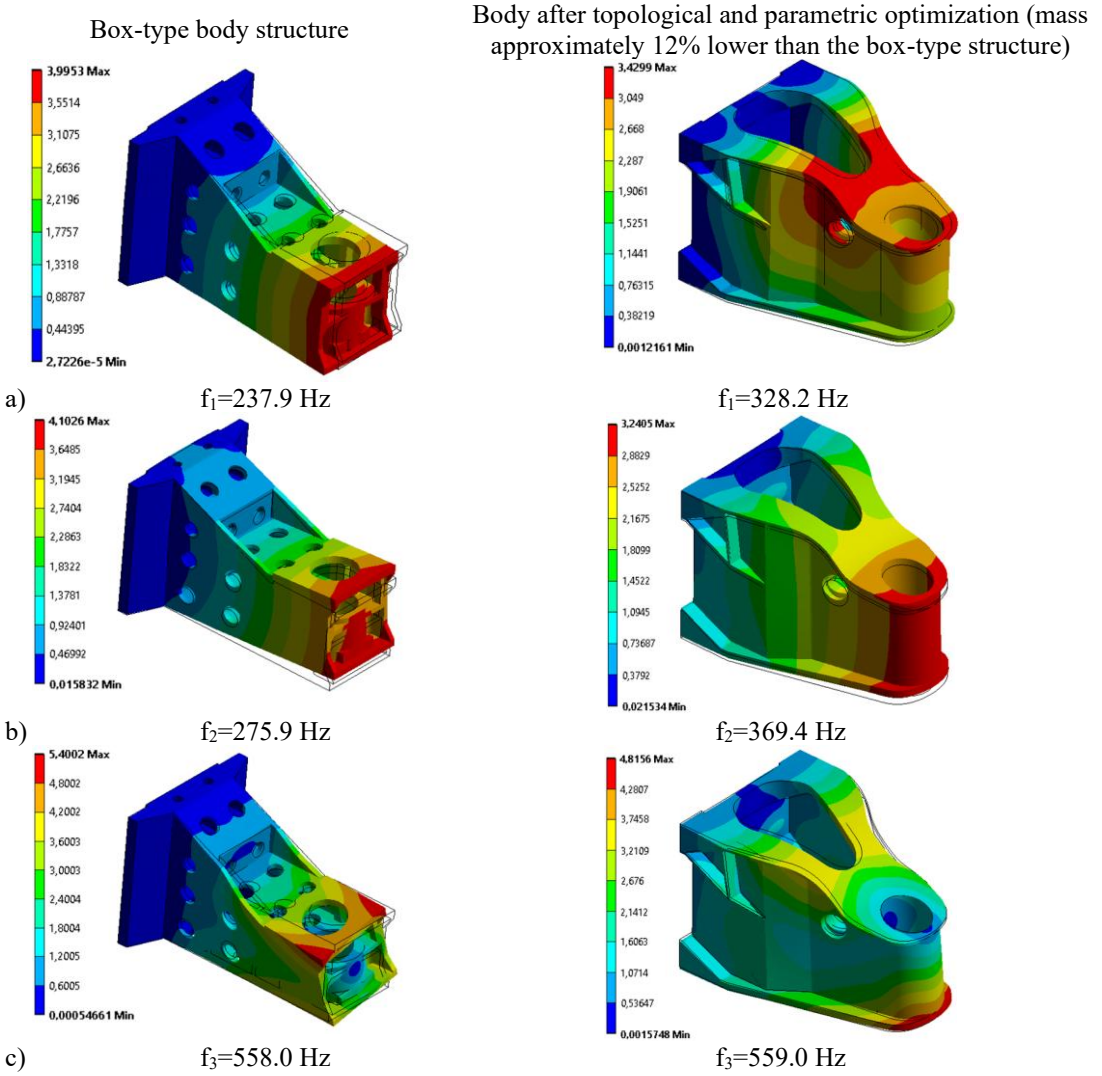

Fig. 11. Comparison of the first three natural frequencies and vibration modes of the box-type headstock and the design after shape and dimensional optimization: (a) first mode of vibration, (b) second mode of vibration, (c) third mode of vibration

4. CONCLUSIONS

The conducted research confirmed the rationale for applying a bionic design approach to the development of a milling headstock body. Inspirations drawn from the structure of toucan and woodpecker beaks enabled the creation of a structure with a high degree of functional sophistication. The application of topology optimization allowed for the development of an internal geometry reduced in terms of mass and reinforced with ribs, resembling natural bone-like structures. Starting from an initial cuboidal geometry representing the overall dimensions of a box-type headstock body, the topology optimization process achieved a mass reduction to 20% while maintaining material continuity.

Since the resulting mass of the headstock body exceeded that of the reference box-type structure, a subsequent parametric optimization was carried out. This process yielded an optimal set of thicknesses for the six main walls, enabling a mass reduction of approximately 12% relative to the box-type headstock body. At the same time, a significant increase in static stiffness was achieved in the X, Y, and Z directions—by 111%, 110%, and 74%, respectively. These improvements translated into increases in the first two natural frequencies by 38% for the first mode and 34% for the second mode. This may be crucial for improving machining accuracy and avoiding resonance during operation. Future work on the headstock body design will focus on developing a physical prototype and experimentally validating the obtained results.

Author contributions: The author confirms sole responsibility for all aspects of the study, including conceptualization, methodology, data collection, analysis, and writing.
Funding source: The author declares that no funds, grants, or other support were received during the preparation of this manuscript.
Conflicts of interest: The author declares no conflict of interest.
Acknowledgements: No acknowledgements to declare.

REFERENCES

1. Bukner S., Dialami F., Ding L., Matthews J. (2015). *Bio-inspired Design to Support Reduced Energy Consumption Via the 'Light Weighting' of Machine System Elements*, International Journal of Modeling and Optimization, 5(1), 82–89. https://doi.org/10.7763/IJMO.2015.V5.441
2. Mechraz, G., Eckert, U., Rentzsch, H., Dani, I., Willocx, M., Duflou, J. R., van Houten, F., Wertheim, R., Ayali, A., Poverenov, E. (2021). *Bio-based design methodologies for products, processes, machine tools and production systems*. CIRP Journal of Manufacturing Science and Technology, 32, 46–60. https://doi.org/10.1016/j.cirpj.2020.11.008
3. Dong A., Guo C., Shen J., Zheng W., Zhang Z. (2024). *Study of the thermal/thermodynamic performance of a bionic flat heat pipe designed to integrate thermal management and bearing capacity*, Thermal Science and Engineering Progress, 49, 102458, 1-12. https://doi.org/10.1016/j.tsep.2024.102458
4. Li, J., Sui, C., Sang, Y., Zhou, Y., Zang, Z., Zhao, Y., He, X., Wang, C. (2024). *A multi-bionic design strategy for modular energy absorption system based on interlocking suture integrated with Bouligand-like arranged perforations*. Thin-Walled Structures, 205, 112553, 1-21. https://doi.org/10.1016/j.tws.2024.112553
5. Huang S., Liu S., Wang D., Takao A., Wu S., Li C., Xiang D., Li C., (2024), *Bionic design and optimization of cutting tools: Applications and processability*, Journal of Manufacturing Processes, 131, 1086–1131.
6. Qiao, Y., Yu, Z., Wang, D. (2025). *Design and optimization of the bionic shark dermal denticle structure for proton exchange membrane fuel cell*. Journal of Power Sources, 647, 237348, 1-12. https://doi.org/10.1016/j.jpowsour.2025.237348
7. Cong Q., Zhang D., Xu J., Chen T., Jin J., Liu C. (2024). *Design the bionic sucker with high adsorption performance based on Sinogastromyzon szechuanensis*, Extreme Mechanics Letters, 73, 102273, 1-10. https://doi.org/10.1016/j.eml.2024.102273
8. Tang Y., Qian X., Yang K., Li X., Huang H., Xu W., Ren L., Liu C. (2025), *Bionic gear design and multiple performance improvements of splash lubrication inspired by fan palm leaves*, International Journal of Heat and Mass Transfer, 242, 126879, 1-19. https://doi.org/10.1016/j.ijheatmasstransfer.2025.126879
9. Huang H., Xian S., Xiong C., Li W., Zhong Y. (2025). *Design and dynamics modeling of a hybrid drive bionic robotic fish*, Biomimetic Intelligence and Robotics, In Press. https://doi.org/10.1016/j.birob.2025.100247
10. Luo, R., Tao, C., Wang, F. (2025). *Design and experimental study of a wire-driven bionic fishtail actuator*. Ocean Engineering, 317, 120087, 1-12. https://doi.org/10.1016/j.oceaneng.2024.120087
11. Shi, X., Chen, T., Zhang, J., Su, B., Cong, Q., Tian, W. (2021). *A review of bioinspired vibration control technology*. Applied Sciences, *11*(22), 10584, 1-14. https://doi.org/10.3390/app112210584

12. Tian J., Li J., Liu G., Shi J., Wu Y. (2025), *Design and performance study of a bionic damping boring bar based on the woodpecker*, CIRP Journal of Manufacturing Science and Technology, 61, 308–323. https://doi.org/10.1016/j.cirpj.2025.06.011
13. Wang, J., Zheng, J., Zhao, Y., Yang, K. (2024). *Structure design and coordinated motion analysis of bionic crocodile robot*. Biomimetic Intelligence and Robotics, 4, 100157, 1-13. https://doi.org/10.1016/j.birob.2024.100157
14. Han D., Hu J., Liu H., Ren L., Yang Q., Cui B. (2025). *Bionic design of an anti-sinking walking wheel for micro tillers and wheel-soil interaction model*, Journal of Terramechanics, 120, 101078, 1-11. https://doi.org/10.1016/j.jterra.2025.101078
15. Mei, X., Liu, C., Li, Z. (2024). *Research progress on functional, structural and material design of plant-inspired green bionic buildings*. Energy & Buildings, 316, 114357, 1-27. https://doi.org/10.1016/j.enbuild.2024.114357
16. An Z., Zhang R., Zhang B. (2024). *Drawing on bionics, a flexible silica fiber paper is designed with high temperature resistance and hydrophobic properties,* Materials Letters, 377, 137441, 1-4. https://doi.org/10.1016/j.matlet.2024.137441
17. Gao L., Deng Y., Liu S., Ren F., Wan M.P., Yang L., Fan J. (2024). *Design and optimization of a bionic-lotus root inspired shell-and-tube latent heat thermal energy storage unit*, International Journal of Heat and Mass Transfer*,* 226, 125437, 1-15. https://doi.org/10.1016/j.ijheatmasstransfer.2024.125437
18. Chen H., Jiang Q., Zhang Z., Wu S., Shen Y., Xu F. (2025). *Structural design and optimization of adaptive soft adhesion bionic climbing robot,* Automation in Construction, 171, 105975, 1-19. https://doi.org/10.1016/j.autcon.2025.105975
19. Han X., Wang Y., Bi S., Meng Y., Zhang L., Jin L., Piao J., Yang X., Jiang C., Gao W. (2025). *Artificial neural network reinforced topological optimization for bionics-based high-performance hydrogen sensor design under multi-physical field coupling*, International Journal of Hydrogen Energy*,* 138, 226–235. https://doi.org/10.1016/j.ijhydene.2025.05.177
20. Su, F., Chen, K., Liu, X., Zhang, K., Ding, X. (2024). *Research of bamboo rat tooth bionic bit structural design and cutting mechanism for CFRP drilling*. Composite Structures*, 334*, 117950, 1-17. https://doi.org/10.1016/j.compstruct.2024.117950
21. McKittrick J., Chen P.-Y., Bodde S.G., Yang W., Novitskaya E.E., Meyers M.A., (2012), *The Structure, Functions, and Mechanical Properties of Keratin*, JOM: Journal of the Minerals, Metals & Materials Society, 64(4), 449–468.
22. Seki Y., Kad B., Benson D., Meyers M.A., (2006), *The toucan beak: Structure and mechanical response*, Materials Science and Engineering *C*, 26, 1412–1420.
23. Wu, C. W., Zhu, Z. D., Zhang, W. (2015). *How woodpecker avoids brain injury*? Journal of Physics: Conference Series*, 628*, 012007, 1-11. https://doi.org/10.1088/1742-6596/628/1/012007
24. Zhu Z.D., Wu C.W., Zhang W., (2014), *Frequency Analysis and Anti-Shock Mechanism of Woodpecker's Head Structure*, Journal of Bionic Engineering, 11(2), 282–287.

Received: October 13th, 2025 / Accepted: December 5th, 2025 / Paper available online: December 20th, 2025